Regularization Reconstruction Method for Imaging Problems in Electrical Capacitance Tomography

Pan Chu [1, 2], and Jing Lei [3]

1. Guangdong Electric Power Design Institute Co., Ltd., China Energy Engineering Group, Guangzhou 510663, China;
2. Institute of Electrical Engineering, Chinese Academy of Sciences, Haidian District, Beijing 100190, China;
3. School of Energy, Power and Mechanical Engineering, North China Electric Power University, Changping District, Beijing 102206, China.

chupandr@126.com (Pan Chu)

Abstract. The electrical capacitance tomography (ECT) is deemed to be a powerful visualization measurement technique for the parametric measurement in a multiphase flow system. The inversion task in the ECT technology is an ill-posed inverse problem, and seeking for an efficient numerical method to improve the precision of the reconstruction images is important for practical measurements. By the introduction of the Tikhonov regularization (TR) methodology, in this paper a loss function that emphasizes the robustness of the estimation and the low rank property of the imaging targets is put forward to convert the solution of the inverse problem in the ECT reconstruction task into a minimization problem. Inspired by the split Bregman (SB) algorithm, an iteration scheme is developed for solving the proposed loss function. Numerical experiment results validate that the proposed inversion method not only reconstructs the fine structures of the imaging targets, but also improves the robustness.

1. Introduction

The ECT technique tries to reconstruct the permittivity distribution in a measurement domain from the given capacitance data via a suitable imaging technique, which has been intensively studied and is regarded to be a promising visualization parametric measurement modality for two-phase or multiphase flow systems.

The performance of the imaging techniques is important for real-world measurement tasks. A range of algorithms, e.g., the linear back-projection (LBP) method [1], the Tikhonov regularization (STR) method [2] and its variations [3, 4], the offline iteration and online reconstruction (OIOR) algorithm [5], the Landweber iteration (LI) algorithm [6-8], the algebraic reconstruction technique (ART) [9], the tensor based imaging technique [10], etc., have been put forward for improve the imaging precision. For existing imaging techniques, however, the reconstruction precision for a complicate target is hardly satisfactory, and seeking for an effective numerical method to improve the imaging quality remains an open problem. Beyond traditional reconstruction methods, naturally, in this paper we introduce a new loss function and an efficient numerical algorithm to improve the reconstruction accuracy, and the main contributions can be presented as follows:

(1) A new loss function that emphasizes the robustness of the estimation and the low rank property of the reconstruction targets is put forward to reformulate the solution of the inverse problem in the ECT reconstruction task into a minimization problem.

(2) Inspired by the SB technique, an iteration technique that integrates the advantages of the fast iterative shrinkage thresholding (FIST) method is developed for the solution of the proposed loss function.

(3) Numerical experiment results validate that the proposed inversion method not only reconstructs the fine structures of the imaging targets, but also improves the robustness.

The remnant of this paper is scheduled as follows. Section 2 reviews the ECT model. We introduce the loss function and the numerical method in Sections 3 and 4, respectively. Section 5 presents numerical experiment results, and Section 6 draws the primary conclusions of the study.

2. Inversion model

The inverse problem in the ECT area tries to reconstruct the permittivity distribution, $\boldsymbol{x}$, from the known sensitivity matrix, $\boldsymbol{A}$, and capacitance value, $\boldsymbol{y}$, under the consideration of the measurement noises, $\boldsymbol{r}$, which can be expressed as the following mathematical model [9]:

$$\boldsymbol{A}\boldsymbol{x} = \boldsymbol{y} + \boldsymbol{r} \tag{1}$$

where the dimensionalities of $\boldsymbol{A}$, $\boldsymbol{x}$, $\boldsymbol{y}$ and $\boldsymbol{r}$ are $m \times n$, $n \times 1$, $m \times 1$ and $m \times 1$, respectively

It is difficult to directly solve equation (1). With the assistance of the TR methodology [2], the solution of equation (1) can be cast into a generalized minimization problem:

$$\min\left\{R(\boldsymbol{x}, \boldsymbol{y}) + \alpha\psi(\boldsymbol{x})\right\} \tag{2}$$

where $R(\boldsymbol{x}, \boldsymbol{y})$ measures the data fidelity; $\psi(\boldsymbol{x})$ means the regularizer and $\alpha > 0$ stands for the regularization parameter.

Equation (2) introduces a generalized optimization problem for the solution of equation (1). However, in order to solve a specific tomography inversion problem, we must settle two problems. On the one hand, how to construct a loss function? On the other hand, how to solve the loss function? In the rest of the paper, we will answer the two questions to achieve the improvement of the reconstruction precision.

3. Loss function

According to equation (2), we must determine the data fidelity term and the regularizer before implementing the image reconstruction.

Beyond the least squares (LS) method that is often employed to measure the data fidelity, with a high sensitivity to outliers contained in the measurement data, in this study we use the absolute value function to measure the data fidelity to improve the robustness of the estimation,, which has the following expression:

$$R(\boldsymbol{x}) = \| \boldsymbol{A}\boldsymbol{x} - \boldsymbol{y} \|_1 \tag{3}$$

where $\| \cdot \|_1$ means the 1-norm.

Studies find that a two-dimensional ECT visual image often has low rank characteristic, and integrating such prior may be helpful for ameliorating the reconstruction quality. The nuclear norm is a powerful approach to impose the low rank constraint. For a two-dimensional image, $\boldsymbol{X}$, the nuclear norm is defined as [11, 12]:

$$\| \boldsymbol{X} \|_* = \sum\nolimits_k \sigma_k \tag{4}$$

where $\sigma_k \geq 0$ is the singular values of the image matrix $\boldsymbol{X}$.

In order to improve the numerical performances of the nuclear norm, the authors in [13] extended the nuclear norm into the weighted nuclear norm, i.e.,

$$\| \boldsymbol{X} \|_{w,*} = \sum\nolimits_i | \boldsymbol{w}_i \sigma_i(\boldsymbol{X}) | \tag{5}$$

where $\boldsymbol{w}_i \geq 0$ are the weighted values and $|\cdot|$ represents an absolute operator.

In this study we use the weighted nuclear norm to serve as a regularizer. Finally, submitting equations (3) and (5) into equation (2) leads to the resulting loss function, i.e.,

$$\min\left\{\| \boldsymbol{Ax}-\boldsymbol{y}\|_1 +\alpha\sum_i |\boldsymbol{w}_i\sigma_i(\boldsymbol{X})|\right\} \tag{6}$$

4. Numerical method

The solution of equation (6) is important. Inspired the SB technique [14], in this work an efficient iteration technique is developed for the solution of equation (6).

With the help of the numerical optimization theory, equation (6) can be reformulated into a constrained minimization problem, i.e.,

$$\begin{cases}\min\left\{\| \boldsymbol{d}\|_1 +\alpha\sum_i |\boldsymbol{w}_i\sigma_i(\boldsymbol{X})|\right\} \\ s.t.\ \boldsymbol{d}=\boldsymbol{Ax}-\boldsymbol{y}\end{cases} \tag{7}$$

Applying the SB technique [14] to equation (7) yields the following sub-problems:

$$\min\left\{\| \boldsymbol{d}\|_1 +\alpha\sum_i |\boldsymbol{w}_i\sigma_i(\boldsymbol{X})|+\frac{\mu}{2}\| \boldsymbol{d}-(\boldsymbol{Ax}-\boldsymbol{y})-\boldsymbol{b}^k\|^2\right\} \tag{8}$$

$$\boldsymbol{b}^{k+1}=\boldsymbol{b}^k-(\boldsymbol{d}^{k+1}-(\boldsymbol{Ax}^{k+1}-\boldsymbol{y})) \tag{9}$$

For the sake of easy computation, applying the alternating optimization strategy to equation (8) leads to the following two decoupled sub-problems:

$$\boldsymbol{d}^{k+1}=\min\left\{\| \boldsymbol{d}\|_1 +\frac{\mu}{2}\| \boldsymbol{d}-(\boldsymbol{Ax}^k-\boldsymbol{y})-\boldsymbol{b}^k\|^2\right\} \tag{10}$$

$$\boldsymbol{x}^{k+1}=\min\left\{\alpha\sum_i |\boldsymbol{w}_i\sigma_i(\boldsymbol{X})|+\frac{\mu}{2}\| \boldsymbol{d}^{k+1}-(\boldsymbol{Ax}-\boldsymbol{y})-\boldsymbol{b}^k\|^2\right\} \tag{11}$$

The solution of equation (10) can be specified as:

$$\begin{aligned}\boldsymbol{d}^{k+1}&=\min\left\{\| \boldsymbol{d}\|_1 +\frac{\mu}{2}\| \boldsymbol{d}-(\boldsymbol{Ax}^k-\boldsymbol{y})-\boldsymbol{b}^k\|^2\right\} \\ &=\text{shrinkage}((\boldsymbol{Ax}^k-\boldsymbol{y})+\boldsymbol{b}^k,1/\mu)\end{aligned} \tag{12}$$

where the operator $\text{shrinkage}(\cdot,\vartheta)=\text{sgn}(\cdot)\max\{|\cdot|-\vartheta,0\}$ is defined as the soft thresholding function with threshold ϑ, and $\text{sgn}(\cdot)$ stands for the sign function.

The solution of the minimization problem in equation (11) is crucial. For easy notation, we rewrite the minimization problem in equation (11) as:

$$\min\{p(\boldsymbol{x})+q(\boldsymbol{x})\} \tag{13}$$

where $p(\boldsymbol{x})=\frac{\mu}{2}\| \boldsymbol{d}^{k+1}-(\boldsymbol{Ax}-\boldsymbol{y})-\boldsymbol{b}^k\|^2$ and $q(\boldsymbol{x})=\alpha\sum_i |\boldsymbol{w}_i\sigma_i(\boldsymbol{X})|$.

Inspired by the successes of the fast iterative shrinkage-thresholding (FIST) algorithm [15], in this study we use it to solve equation (13), which has the following computational flowchart:

Step 1. The initial value and the algorithmic parameters are given.

Step 2. Begin the iteration by setting $L_1=\boldsymbol{x}_0$ and $t_1=1$. For the iteration index j $(j\geq 1)$, implement the following iteration until a predetermined stopping condition is met.

a) $\boldsymbol{x}_j=s(\boldsymbol{L}_j)$, where $s(\cdot)$ is specified as:

$$s=\min\left\{\frac{\ell}{2}\| \boldsymbol{x}-(\boldsymbol{L}_j-(1/\ell)\nabla p(\boldsymbol{L}_j))\|^2 +q(\boldsymbol{x})\right\} \tag{14}$$

where $\nabla p(\boldsymbol{x}_{j-1})$ represents the gradient of function $p(\boldsymbol{x})$.

b) $t_{j+1} = \left(1+\sqrt{1+4t_j^2}\right)/2$

c) $\boldsymbol{L}_{j+1} = \boldsymbol{x}_j + (\boldsymbol{t}_j - 1)(\boldsymbol{x}_j - \boldsymbol{x}_{j-1})/\boldsymbol{t}_{j+1}$

The resulting computational flowchart for solving the minimization problem in equation (7) is presented as follows:

Step 1. Provide the initial value and the algorithmic parameters, and set $k = 1$.

Step 2. Update the variable $\boldsymbol{d}$ by equation (12).

Step 3. Update the variable $\boldsymbol{x}$ via solving equation (11) using the FIST technique.

Step 4. Update the variable $\boldsymbol{b}$ by equation (9).

Step 5. If a predetermined stopping condition is satisfied, stop iterations and output the result; or, set $k \leftarrow k+1$, skip to Step 2.

For easy notation, in this study we called the aforementioned iteration scheme as the regularization reconstruction (RR) method.

5. Numerical experiments and discussions

Numerical experiments are performed to test the RR algorithm, and the reconstruction precision is evaluated in comparison with several competitors, e.g., the LBP technique, the OIOR method, the LI technique and the TR method.

A square sensor is used to execute simulation experiments, and it holds 12 electrodes. We use 32×32 pixels for the visualization presentation of an image.

In the RR algorithm, the termination condition of the iteration is defined by:

$$\frac{\| \boldsymbol{x}^{k+1} - \boldsymbol{x}^{k} \|}{\| \boldsymbol{x}^{k} \|} \leq 1 \times 10^{-4} \tag{15}$$

where k means the iteration index.

We use the noisy data to assess the robustness of the RR algorithm, and the noise level (NL) is defined in [10]. Meanwhile, we use the image error (IE) [10] to quantitatively appraise the reconstruction accuracy for these competing methods.

5.1. Case 1

We test the RR method and the other competing methods on three noise-free tomographic targets which are shown in Figure 1. The regularization parameter for the TR technique is empirically selected 0.003. The relaxation factor for the LI technique is 1 and the number of iterations corresponds to the minimum RE for the fair comparison. In the RR technique, $\alpha = 1$, and the weighted values are $\boldsymbol{w}_i = 1/(|\boldsymbol{\sigma}_i(\boldsymbol{X}^{k-1})|^4 + 10^{-10})$. The resulting reconstruction images from the competing algorithms are presented in Figures 2-6. We illustrate the IEs for the competitors in Table 1.

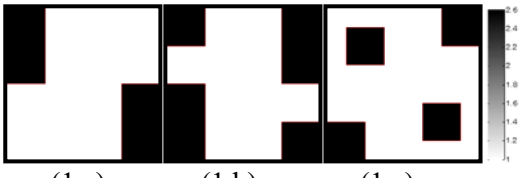

(1.a) (1.b) (1.c)

Figure 1. Tomographic targets

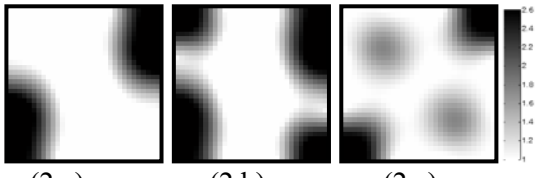

(2.a) (2.b) (2.c)

Figure 2. Images reconstructed by the LBP algorithm

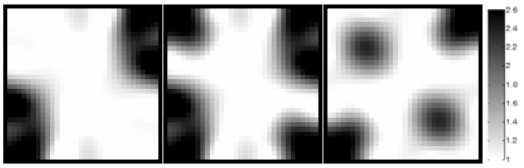

(3.a) (3.b) (3.c)

Figure 3. Images reconstructed by the TR algorithm

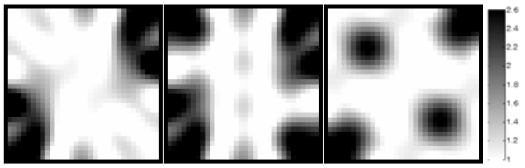

(4.a) (4.b) (4.c)

Figure 4. Images reconstructed by the OIOR algorithm

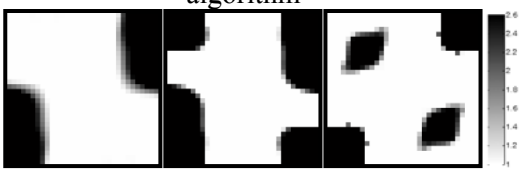

(5.a) (5.b) (5.c)

Figure 5. Images reconstructed by the LI algorithm

(6.a) (6.b) (6.c)

Figure 6. Images reconstructed by the RR algorithm

Table 1. Image errors (%)

Algorithms	Figure 1(a)	Figure 1(b)	Figure 1(c)
LBP	16.15	18.27	28.05
TR	16.24	17.33	22.26
OIOR	17.94	17.24	20.64
LI	12.20	11.44	14.36
RR	9.31	9.93	10.95

Qualitative analysis indicates that the RR technique simultaneously emphasizes the robustness of the estimation and the low rank property of the tomographic targets, which will be helpful for the improvement of the precision of the reconstruction images. In fact, in Figures 2-6, we can observe that the resulting images reconstructed by the RR algorithm are better than the other competitors, e.g., the LBP technique, the OIOR algorithm, the LI technique and the TR method, and the spatial resolutions are improved. For the quantitative comparison, it is observed from Table 1 that the IEs of the RR technique are smallest among all competing algorithms. These qualitative and quantitative comparison results validate the effectiveness of the RR technique on improving the reconstruction accuracy.

5.2.Case 2

In this case, we use the noisy capacitance data to quantitatively test the robustness of the RR algorithm. The algorithmic parameters for the RR algorithm are identical to Section 5.1. Figures 7 and 8 show the results reconstructed by the RR algorithm under the NLs of 5% and 10%, respectively. We list the IEs under different NLs in Table 2 for the quantitative comparison.

(7.a) (7.b) (7.c)

Figure 7. Reconstructed images by the RR algorithm when the NL is 5%

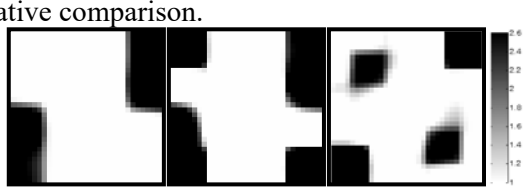

(8.a) (8.b) (8.c)

Figure 8. Reconstructed images by the RR algorithm when the NL is 10%

Table 2. Image errors under different NLs (%)

NLs	Figure 1(a)	Figure 1(b)	Figure 1(c)
5%	10.75	9.99	11.81
10%	10.79	10.66	11.93

The consideration of the noisy influences on imaging results in the proposed loss function will be helpful for increase the robustness. In Figures 7 and 8, the RR algorithm shows excellent robustness, and the reconstruction results under different NLs are acceptable. Besides, the IEs listed in Table 2 validate the capability of the RR method in coping with the noisy measurements.

6. Conclusions

In this work, we improve the reconstruction quality in the ECT instrument by introducing new numerical strategies. Such improvements are derived from two aspects. One the one hand, a loss function that focuses on the robustness of the estimation and the low rank property of the reconstruction targets is put forward to model the ECT inverse procedure. On the other hand, the SB technique and the FIST algorithm are incorporated to create an efficient numerical scheme to solve the proposed loss function. Qualitative evaluation results and visual comparisons from numerical experiments confirm that the proposed algorithm not only reconstructs the details of the tomographic targets, but also gives rise to the improvement of the robustness.

References

[1] Xie C G, Huang S M, Hoyle BS, Thorn R, Lenn C, Snowden D and Beck MS 1992 *IEE Proceedings G-Circuits, Devices and Systems* **139** 89
[2] Tikhonov A N and Arsenin V Y 1977 *Solution of ill-posed problems* (New York, V.H. Winston & Sons)
[3] Lei J, Qiu J H and Liu S 2015 *Applied Mathematical Modelling* **390** 6925.
[4] Soleimani M, Lionheart W R B 2005 *Measurement Science and Technology* **16** 1987
[5] Liu S, Fu L, Yang W Q, Wang H G and Jiang F 2004 *IEE Proceedings-Science, Measurement and Technology* **151** 195
[6] Landweber L 1951 *American Journal of Mathematics* **73** 615
[7] Yang W Q, Spink D M, York T A and McCann H 1999 *Measurement Science and Technology* **10** 1065
[8] Jang JD, Lee SH, Kim K Y and Choi B Y 2006 *Measurement Science and Technology* **17** 1909
[9] Yang W Q and Peng L H 2003 *Measurement Science and Technology* **14** L1
[10] Lei J, Liu W Y, Liu S and Wang X Y 2015 *Flow Measurement and Instrumentation* **41** 104.
[11] Candès E J and Tao T 2010 *IEEE Transactions on Information Theory* **56** 2053
[12] Candès E J and Recht B 2009 *Foundations of Computational Mathematics* **9** 717
[13] Cui Z, Zhang D, Wang K, Zhang H, Li N and Zuo W 2015 *Mathematical Problems in Engineering* **2015** 1
[14] Goldstein T and Osher S 2009 *SIAM Journal on Imaging Sciences* **2** 323
[15] Beck A and Teboulle M 2009 *SIAM Journal on Imaging Sciences* 2 183